SAND2010-0724C

Determination of Dihedral Angles at Grain Boundary Triple Junctions

Michael Chandross[a], Elizabeth A. Holm[b]

Sandia National Laboratories, Albuquerque, NM 87185-1411 U.S.A.

[a]mechand@sandia.gov, [b]eaholm@sandia.gov

Keywords: microstructure, triple junctions, dihedral angles, modeling and simulation.

Abstract. With the advent of computer simulations and experimental techniques such as EBSD, digitized microstructures are becoming pervasive. Measuring grain junction angles in these microstructures is complicated by the implicit and discrete nature of the grain boundaries. We have developed a high-throughput, robust method to measure realistic grain junction angles in planar discretized microstructures. Using this method, we characterize the difference between planar sections of 2D columnar and 3D equiaxed grain structures.

Introduction

Most microstructures that are acquired or analyzed by computers are digitized: they consist of a regular array of 2D pixels or 3D voxels, where the pixels/voxels may contain information such as grain membership or orientation. This is true both of computer simulated microstructures (generated by Monte Carlo Potts, cellular automaton, and some Phase Field models) and experimental images (particularly from EBSD microscopy, but also some digital image processing packages).

In digitized microstructures, grain boundaries are implicit; they occur where unlike pixels/voxels meet. Further, grain boundaries confirm to the pixel/voxel lattice and may be quite rough. Because of this discretization, the tangent to the boundary at a grain junction is not uniquely defined, so there is no definition of the "correct" junction angle. For example, in the triple junction shown in Fig. 1(a), the triple junction angle θ calculated by examining only first neighbor pixels is 180°, which is far from the angle of 90° calculated by a linear fit to the two incident boundaries.

In this paper, we present a robust method to measure realistic grain junction angles in planar discretized microstructures. This method is applicable to experimental and simulated structures. As an example, we then apply this method to characterize the difference between planar sections of 2D columnar and 3D equiaxed grain structures.

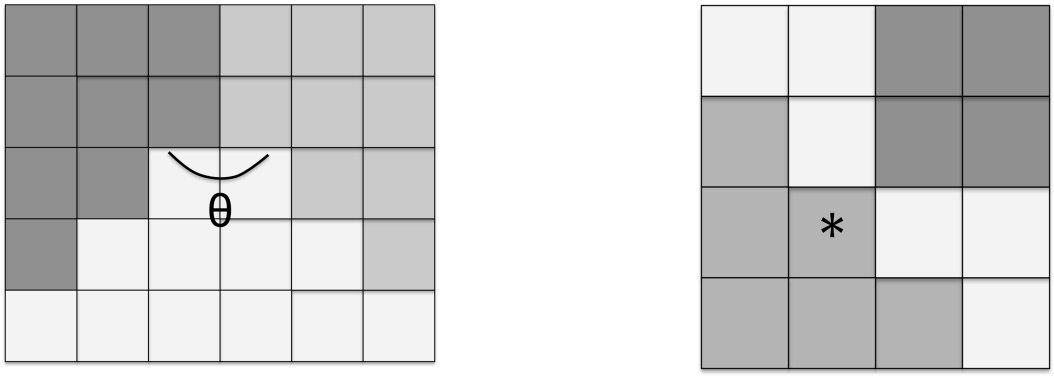

(a) (b)

Figure 1. Grain junctions in discretized microstructures, where pixel color correlates with grain membership. (a) A triple junction with dihedral angle θ. Note that the measured angle varies considerably depending on the number of boundary segments considered. (b) A quad junction where the light grain is divided by the two darker grains. The pixel indicated with an asterisk (*) is a boundary site with only one unlike neighbor grain type (light gray) that nonetheless represents a grain junction.

Method

An accurate method for determining an approximate tangent to a discretized grain boundary involves calculating some kind of curve fit to the boundary. In order to arrive at such a fit, it is first necessary to acquire a representation of the boundary. This information is only implicitly present in a discretized microstructure; a boundary site is a pixel that has one or more unlike neighbor pixels. Thus, we can classify boundary sites according to the number of unlike neighbor pixels. A pixel with one unlike neighbor defines a grain boundary, except in the special case shown in Fig. 1(b), which represents a quad junction. Boundary sites that have three or four distinct grains among their neighbor pixels are triple or quad junctions, respectively.

Individual grain boundaries are mapped out as follows. First, all boundary sites are identified as one of the types defined above. For each pair of grains, the boundary is followed (i.e. by moving to the next boundary site bounded by the appropriate grains and keeping track of the direction of movement) until a terminal triple/quad junction is reached. This maps out a discrete grain boundary in space; an example of such a boundary is shown in Fig. 2.

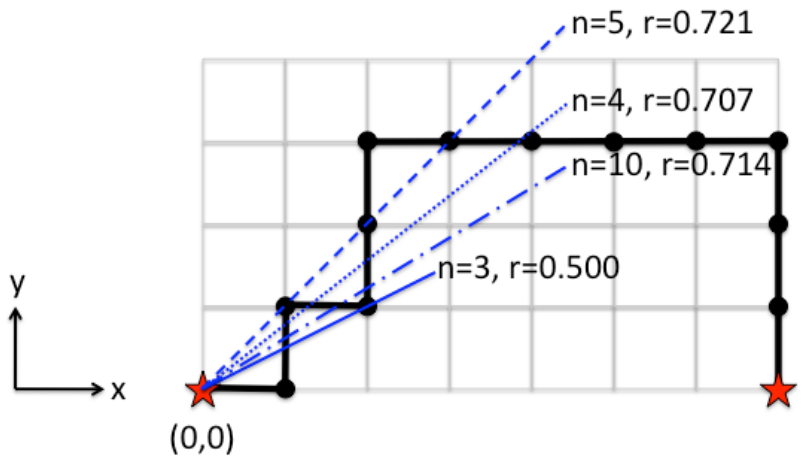

Figure 2. A discretized boundary resulting from the procedure described in the text. Triple/quad points are denoted by stars; the fitting points along the boundary are dots; the underlying lattice of voxels is outlined in gray; and the grain boundary is shown as a heavy line. Also shown are linear fits, computed using equation (2), to n = 3 (solid light line), 4 (dotted line), 5 (dashed line), and 10 (dot-dashed line) points, as well as Pearson's correlation coefficient r for each fit.

A best linear fit is calculated for each boundary using a linear regression algorithm with one restriction – namely that the intercept is forced to be at x=y=0 (i.e. at the triple/quad point) so that all grain boundaries will intersect at a single point. Recall that the correlation coefficient χ^2 for a linear fit of the form $y = ax$ to a series of points (x_i, y_i) is defined by

$$\chi^2 = \sum_{i=1}^{n} (y_i - ax_i)^2 \tag{1}$$

where n is the number of points fit, and a is the slope of the line, i.e. $a = \tan^{-1}\theta$ where θ is the angle of the line with respect to the x-axis; note that $\theta \leq 180°$. Minimization of χ^2 with respect to a gives

$$a = \frac{\sum_{i=1}^{n} x_i y_i}{\sum_{i=1}^{n} x_i^2} \tag{2}$$

Examples of linear fits to n boundary points are shown by the dashed lines in Fig. 2.

For a boundary consisting of n discrete segments, there are n possible linear fits to the boundary. Because the linear regression algorithm relies on minimization of χ^2, this parameter is not useful to determine which of the n possible linear fits is the most accurate. Instead we calculate Pearson's

correlation coefficient r [1] as the relevant goodness-of-fit parameter. This coefficient is calculated by dividing the covariance of two variables, cov(x,y), by the product of their standard deviations, σ_x and σ_y. For a series of points (x_i,y_i), r is given by

$$r = \frac{\mathrm{cov}(x,y)}{\sigma_x \sigma_y} = \frac{\sum_{i=1}^{n}(x_i - \bar{x})(y_i - \bar{y})}{\sqrt{\sum_{i=1}^{n}(x_i - \bar{x})^2}\sqrt{\sum_{i=1}^{n}(y_i - \bar{y})^2}} \tag{3}$$

where $\bar{x}$ is the mean x value and $\bar{y}$ is the mean y value. Pearson's correlation coefficient determines the amount of correlation between two variables. In this case, $|r|$ determines how reasonable a linear fit is to a given segment. As the length increases from 1 to n for a given boundary, $|r|$ starts at 1.0 (since a linear fit to a segment of length 1 is, by definition, exact), and then generally drops to low values for extremely short segments. As the boundary length increases, $|r|$ rapidly increases, remains high and then decreases as the boundary starts to curve. We take the best linear fit as the largest value of $|r|$ before the decrease. Figure 2 shows these trends in the four fits pictured, and Fig. 3 gives a complete plot of $|r|$ versus n for a representative boundary in the microstructures studied here.

This fitting procedure is repeated for all three or four grain boundaries at a given triple or quad point, respectively, to determine the best fit tangent lines for each boundary. Angles between these tangents can now be easily calculated, and the procedure is repeated for all remaining triple and quad junctions.

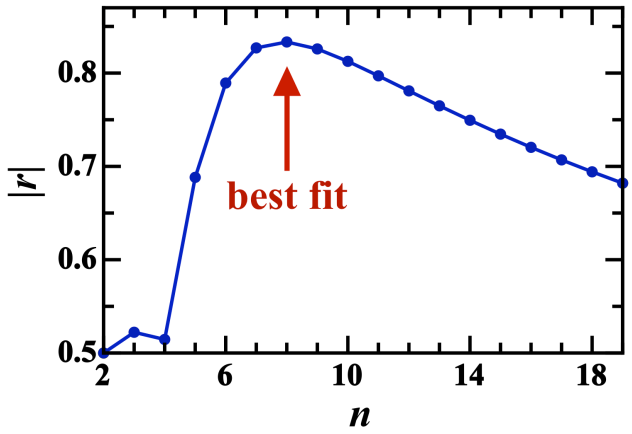

Figure 3. Pearson's correlation coefficient |r| as a function of number of grain boundary segments in the fit n for a representative grain boundary in the microstructures studied here. The best fit, determined by the maximum value of |r| before the steady decrease, is indicated by the arrow.

Results and Discussion

As an example of the usefulness of this method, we apply it to examine the difference between cross-sections of 3D equiaxed microstructures and true 2D columnar microstructures, both generated by Monte Carlo Potts model grain growth [2-5]. The 3D system is a periodic 100x100x100 site cubic lattice evolved from an initially random structure under appropriate conditions to approximate isotropic grain growth (simulation temperature $T = 1.5$, cubic lattice with first, second and third neighbor interactions). After evolution for 100 timesteps, we calculated the average grain radius, R. The grain junction angle calculation was then performed for a series of 2D slices of the microstructure separated by R in order to improve statistics without introducing artificial correlations by analyzing slices that are close to each other.

The distribution of grain junction angles for the 2D slices of the 3D microstructure is shown in Fig. 4(a). The distribution is approximately Gaussian and peaked near 120°, as expected for a regular distribution of triple junction angles in a plane [6]. However, the distribution also shows sharp peaks at 18°, 45°, 63°, 90°, 117°, 135°, 153°, 162°, and 180°. These peaks are spurious and caused by short boundary segments in the 3D cross-sections, as indicated by Fig. 4(b)-(d), which show the angular distributions when short boundary segments are systematically removed from the

system. When we consider only boundaries that contain at least four segments, the spurious peaks disappear (except for a small peak at 90°, which is expected in this square lattice).

Two-dimensional slices of 3D microstructures contain many small grains, thus short boundaries, since all cross sections of a 3D equiaxed grain are generally smaller than the nominal grain size. The number of curve fits that a boundary can be tested against is no more than the number of boundary segments, n. The limited number of fits means that only a limited number of tangent angles can be measured for short boundaries; those disproportionately sampled angles show up as peaks in Fig. 4(a).

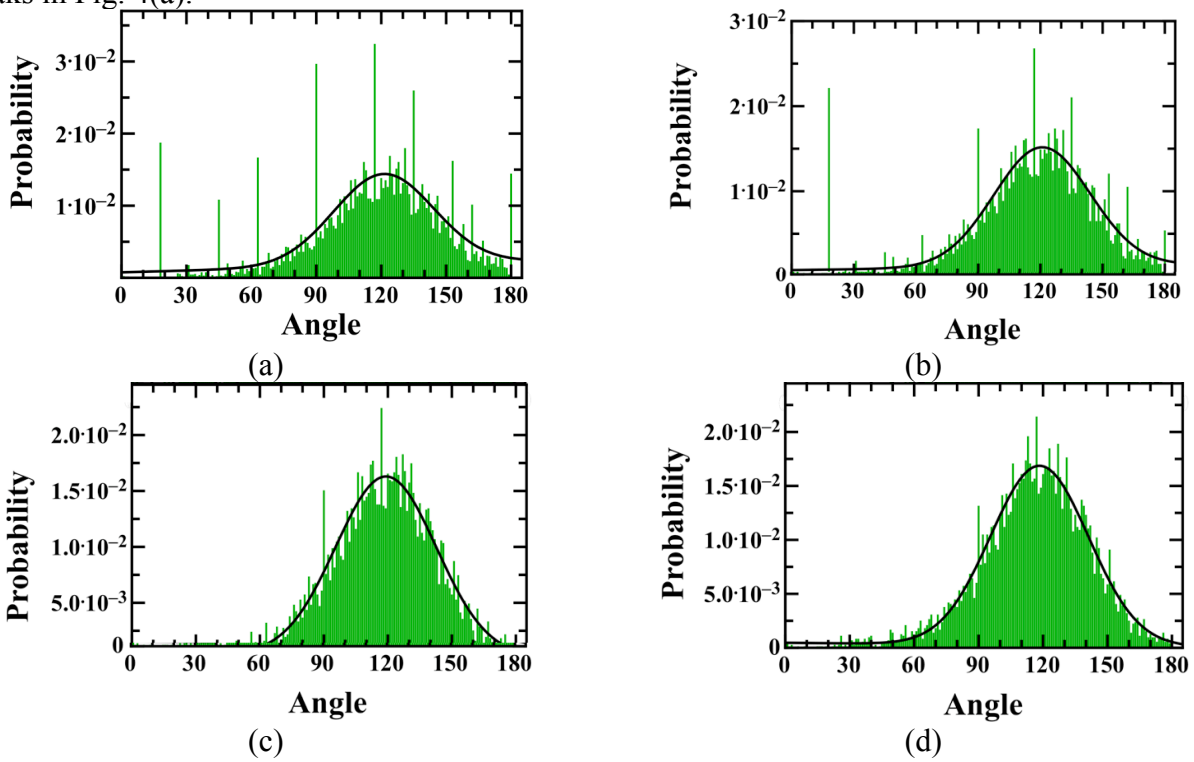

Figure 4. A representative distribution of grain junction angles for a 3D simulated polycrystal using the method described in the text. Distributions are given for (a) the raw microstructure including all boundaries, and with minimum boundary lengths restricted to (b) 2, (c) 3, and (d) 4 segments. The solid dark lines show best fits to a Gaussian distribution; the mean is approximately 120° in each case.

Figure 5 shows the grain junction angle distribution for a 2D polycrystal, evolved using the same Monte Carlo Potts model for grain growth, grown to the same average grain size R as the 3D system, this time on a periodic 1000x1000 two-dimensional square lattice at $T = 2.0$. We have chosen this lattice size to match sample size for the 2D and 3D systems.

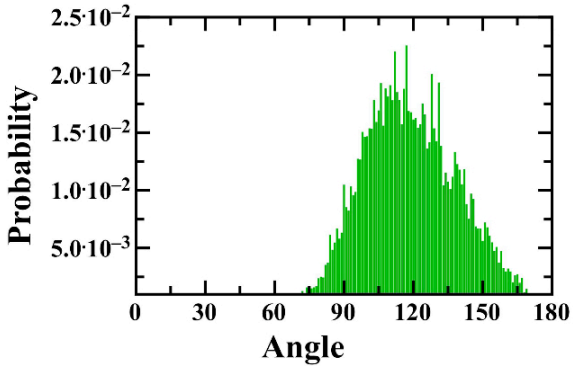

Figure 5. Grain junction angle distribution for a 2D grain growth simulation. The distribution was calculated with a minimum boundary length of 4 segments. Note the difference in distribution shape when compared to the data for 3D cross sections shown in Fig. 4.

Unlike the 3D angle distribution, the 2D distribution is not symmetric and is skewed towards higher angles. The mean angle remains 120°, but the distribution is peaked at a somewhat lower

angle. The distribution is also narrower than in 3D, as expected; however, there is substantial spread in the grain junction angles about the mean of 120°. Recall that in a 2D, perfectly isotropic, continuum polycrystal, all triple junction angles should be 120° [7]. The fact that there is a spread of grain junction angles suggests several possibilities. First, it is impossible to exactly map a 120° angle onto a square lattice; grain junction configurations will encompass a variety of mappings, each with slightly different angles. Second, the Potts model used to generate the 2D microstructure is well known to exhibit anisotropy due to lattice effects [8], resulting in a tendency for grain boundaries to lie along low-index directions of the square lattice. Finally, in the Potts model, there is a finite grain junction equilibration time, in contrast to front-tracking or vertex grain growth models. Thus, grain junctions need not instantaneously maintain their equilibrium angles, and a spread of angle is possible at any given time.

Nevertheless, it is clear that the triple junction angle distribution can be used to differentiate between an equiaxed, 2D microstructure that is a slice of a 3D structure and one that is truly two-dimensional, i.e. a columnar microstructure.

Conclusions

Accurate measurement of dihedral angles between grain boundary junctions can be a valuable tool for analysis of both simulated and experimental microstructures. These angles provide unique signatures of the accuracy of grain growth simulations, energetic anisotropy of grain boundaries, and microstructural dimensionality. However, these angles are difficult to determine because tangents to discretized boundaries are poorly defined.

We have developed a method that can accurately calculate grain junction angles for discretized experimental and simulated microstructures. We have tested the model by comparing cross-sections of 3D microstructures with true 2D, columnar microstructures. We have found that the grain junction angle distribution varies sufficiently to utilize it as a metric to differentiate a columnar structure from the cross-section of an equiaxed structure by analyzing planar micrographs. Future work will include analysis of experimental microstuctures, as well as more quantitative measures of the differences between columnar and equiaxed samples.

Acknowledgements

Sandia is a multi-program laboratory operated by Sandia Corporation, a Lockheed Martin Company, for the United States Department of Energy's National Nuclear Security Administration under contract DE-AC0494AL85000. This work was supported by the DOE Office of Basic Energy Sciences and Sandia's Laboratory Directed Research and Development program.

References

[1] J. L. Rodgers, W. A. Nicewander, American Statistician 42 (1988) 59-66.
[2] M. Anderson, G. Grest, D. Srolovitz, Phil. Mag. B 59 (1989) 293-329.
[3] M. Anderson, D. Srolovitz, G. Grest, P. Sahni, Acta Metallurgica 32 (1984) 783-791.
[4] M. Miodownik, Monte Carlo Potts Model, in: K. G. F. Janssens, D. Raabe, E. Kozeschnik, M. Miodownik, B. Nestler (Eds.), Computational Materials Engineering: An introduction to microstruture evolution, Elsevier Academic Press, London, 2007, pp. 47-108.
[5] A. Rollett, P. A. Manohar, The Monte Carlo Method, in: D. Raabe, F. Roters, F. Barlat, L.-Q. Chen (Eds.), Continuum Scale Simulation of Engineering Materials, Wiley-VCH, Weinheim, Germany, 2004, pp. 77-114.
[6] D. Harker, E. R. Parker, Trans. ASM 34 (1945) 156-201.
[7] C. S. Smith, Grain shapes and other metallurgical applications of topology, in: Metal Interfaces, ASM, Cleveland, OH, 1952, pp. 65-108.
[8] E. Holm, J. A. Glazier, D. Srolovitz, G. Grest, Physical Review A 43 (1991) 2662-2668.